Advances in Nano Research, *Vol. 17, No.1 (2024) 1-8*
https://doi.org/10.12989/anr.2024.17.1.001

Static stability analysis of graphene origami-reinforced nanocomposite toroidal shells with various auxetic cores

Farzad Ebrahimi*[1], Mohammadhossein Goudarzfallahi[2] and Ali Alinia Ziazi[2]

[1]*Department of Mechanical Engineering, Faculty of Engineering, Imam Khomeini International University, Qazvin, Iran*
[2]*Mechanical Engineering Department, Science and Research branch, Islamic Azad University, Tehran, Iran*

(*Received December 29, 2018, Revised January 17, 2021, Accepted May 11, 2021*)

Abstract. In this paper, stability analysis of sandwich toroidal shell segments (TSSs) with carbon nanotube (CNT)-reinforced face sheets featuring various types of auxetic cores, surrounded by elastic foundations under radial pressure is presented. Two distinct types of auxetic structures are considered for the core, including re-entrant auxetic structure and graphene origami (GOri)-enabled auxetic structure. The nonlinear stability equilibrium equations of the longitudinally shallow shells are formulated using the von Kármán shell theory, in conjunction with Stein and McElman approximation while considering Winkler–Pasternak's elastic foundation to simulate the interaction between the shell and elastic foundation. The Galerkin method is employed to derive the nonlinear stability responses of the shells. The numerical investigations show the influences of various types of auxetic-core layers, CNT-reinforced face sheets, as well as elastic foundation on the stability of sandwich shells.

Keywords: carbon nanotube-reinforced composite; elastic foundation structures; radial load; stability analysis; toroidal shell segment; various auxetic

1. Introduction

Auxetic materials are gaining significant attention for research and application in various industries due to their lightweight and exceptional ability to absorb the impact impulses they are subjected to. Compression and shear resistance, energy absorption, low frequency and energy harvesting, and high damping resistance are only some of the mechanical attributes these metamaterials have been shown to improve (Ebrahimi 2019). Advanced composite materials can be developed by integrating an auxetic core layer into a sandwich-structured composite, enhancing its static and dynamic load-carrying capacity. This innovation proves highly beneficial in diverse applications, including civil engineering, aerospace engineering, and energy absorption systems. Numerous previous studies have investigated the mechanical performance of plate and shell structures incorporating auxetic cores. Ebrahimi *et al*. (2023) investigated the vibration analysis of a composite cylindrical shell comprising an auxetic core supported by an elastic foundation subjected to axial compression and external excitation. The study used Donnell's improved shell theory, Volmir's assumption, and Galerkin's and Runge-Kutta's methods for dynamic analysis. Mahinzare *et al*. (2023) studied the nonlinear vibrations of an intelligent plate with an auxetic core and piezoelectrically-driven multiscale nanocomposite layers. They used higher-order shear deformation theory to examine the smart plate's behavior. The plate's equations were derived from Hamilton's principle, Maxwell's law, and von Karman's nonlinearity. The governing equations for the sandwich plate were discretized using differential quadrature under various boundary conditions. Dabbagh *et al*. (2023) investigated the wave propagation analysis of smart auxetic-core composite beams in which the material parameters of the auxetic ply were obtained using an analytical micromechanical method. Seyfi *et al*. (2021) studied torsional vibration analysis of non-circular nanorods in auxetic honeycombs, using Eringen's nonlocal elasticity theory (ENET) to account for scale effects. Kinematic relations were derived from Hamilton's principle and governing equations of nanorods under various boundary conditions were solved analytically.

Carbon nanotubes (CNTs) are highly suitable for enhancing composite materials because of their outstanding thermal, mechanical, and electrical characteristics. When incorporated as fibers, they can be distributed within a polymeric matrix in a manner that is either uniform (UD) or functionally graded (FG). Shen (2014) presented a post-buckling analysis for FG-CNTRC cylindrical shells and employed a perturbation technique to obtain the buckling and post-buckling behavior of the shell. Sofiyev *et al*. (2022) studied buckling in conical shells reinforced by CNTs under hydrostatic pressure and axial compression on an elastic foundation. They used the first-order shear deformation shell theory (FSDST) to derive the governing equations. Three CNT distributions (uniform, V, and X-type) were considered. Stability equations were solved via the Galerkin method to find combined buckling loads (CBLs). Shen (2011) studied the post-buckling analysis of CNT-reinforced cylindrical shells subjected to lateral load in a thermal environment. The governing equations were obtained using a higher-order shear deformation theory and incorporating von Kármán-type kinematic nonlinearity. Buckling loads and post-buckling equilibrium paths were

*Corresponding author, Ph.D., Professor,
E-mail: febrahimy@eng.ikiu.ac.ir

ISSN: 2287-237X (Print), 2287-2388 (Online)

determined using a perturbation technique.

Graphene, discovered in 2004, is a two-dimensional material that is just one atom thick and has a high ratio of surface area to thickness. Carbon atoms are joined by bundles to form a graphene sheet's structure, which repeats as a hexagon. Excellent mechanical strength, heat conduction, and electrical conduction have all been demonstrated by this nanostructure. The mechanical properties of the graphene layer have been observed, revealing that it is even more rigid than stainless steel in two dimensions. In the majority of simulations, the graphene sheet's elasticity modulus is reported to be around 1 TPa (Ebrahimi and Dabbagh 2022, Ebrahimi 2015). As a result of such intriguing characteristics, graphene may be considered a highly promising option for the reinforcement of composites, leading to the development of a new type of nanocomposite material identified as FG graphene-reinforced composite (FG-GRC) (Shen 2017). Subsequently, research was conducted on the thermal and mechanical properties of laminated plates and shells made from FG-GRC (Shen and Xiang 2018, Kiani 2018a, b, Ebrahimi and Barati 2018, 2019, Ebrahimi *et al*. 2019, 2020, Ebrahimi and Dabbagh 2019)

Recently, there has been a surge in the popularity of utilizing the traditional paper craft of origami, which involves folding paper (the Japanese terms 'ori' meaning 'fold' and 'gami' meaning 'paper'). This resurgence is particularly notable in the creation of mechanical metamaterials. The folding of basic two-dimensional thin-film materials makes it possible to convert them into intricate three-dimensional structures with distinctive and adjustable mechanical characteristics. These properties include flexibility, tunable Poisson's ratio, and adjustable stiffness (Zhai *et al*. 2021). Motivated by the Miura-origami metamaterial and graphene origami (GOri), a novel category of GOri-enabled metallic metamaterials (GOEAMs) that possess superior characteristics has been developed. These materials exhibit tunable NPR and improved mechanical properties. The research indicates that the adjustability of NPR is attainable by altering the content of graphene, graphene folding degree, and temperature. Additionally, micromechanical models assisted by genetic programming (GP) have been developed to predict the mechanical characteristics of the GOEAMs precisely (Zhao *et al*. 2022a, b). Zhao *et al*. (2022b) studied beams' dynamic responses and free vibration behavior composed of a unique combination of GOEAMs. These beams exhibit an auxetic property, and their dynamic characteristics are effectively controlled by the content of graphene as well as the folding degree of GOri, both of which vary across the thickness of the beams. The research findings demonstrated that the inclusion of GOri allows for a high degree of tunability in the structural vibration characteristics of the beams. The findings of this observation offer vital insights into prospective structural applications, particularly within the field of aeronautical engineering, which ultimately leads to significantly improved dynamic structural performance. In another study, Zhao *et al*. (2022c) examined the buckling and post-buckling characteristics of GOEAM beams. They noted FG beams' adjustable buckling and post-buckling features, which provide valuable insights for designing advanced structures. Ebrahimi *et al*. (2023) employed the Timoshenko beam theory in their research to investigate the propagation of waves in auxetic metamaterial beams featuring FG GOri. The study delves into different distribution patterns and utilizes Hamilton's principle to formulate kinetic equations. The research identifies key aspects through thorough analysis and comparison by comparing a range of parameters, such as graphene distribution, folding degree of GOri, temperature, wave number, and elastic foundation coefficients. Mahinzare *et al*. (2024) studied the nonlinear vibrational behavior of a smart multiscale hybrid sandwich plate with FG-GOri using geometrically von Karman factors and Mindlin plate theory. Electro-elastic layer properties were determined by the Halpin-Tsai model and the rule of mixing. The governing equations were derived employing Hamilton's principle, Maxwell's law, and von Karman factors. Ebrahimi and Ahari. (2024) investigated the buckling behavior of a composite material with magnetostrictive face sheets and GOri-enabled features. Eringen's nonlocal theory was used to quantify the small-scale parameter, and higher-order sinusoidal shear deformation theory was used to formulate the governing equation. The Galerkin solution method solves the governing equation while considering various boundary conditions.

Toroidal shell segments (TSSs) are extensively used in various engineering applications, including aeronautical, underwater, and civil structures. Buckling analysis for these types of shells of revolution, composed of modern composite materials, has received significant attention in the last few years. Nguyen *et al*. (2023) investigated the buckling and nonlinear post-buckling analysis of TSSs with honeycomb auxetic-core layer and GRC coatings subjected to torsional loads. They employed von Karman-Donnell shell theory and the Stein and McElman approximations (Stein and McElman 1965) to derive the equilibrium equations for shells with longitudinally shallow curvature, surrounded by an elastic foundation. They utilized the Galerkin procedure to present the governing equations. Tien *et al*. (2022) studied honeycomb auxetic-core sandwich TSSs with CNT-reinforced face sheets under radial pressure. They analyzed nonlinear buckling using von Kármán-Donnell theory and Stein and McElman approximations, obtaining pre-buckling and post-buckling responses via the Galerkin procedure. In a similar research, Phuong *et al*. (2023) investigated the buckling and post-buckling behavior of TSSs composed of a honeycomb auxetic core and graphene-reinforced face sheets subjected to radial loads. Different types of graphene distribution were considered for the laminated face sheets using the Galerkin method. Hieu and Tung (2020) studied the buckling and post-buckling analysis of CNRC TSSs subjected to combined thermal and mechanical loads with UD and FG types of CNT distribution. Nam *et al*. (2022) analyzed nonlinear buckling in honeycomb auxetic-core sandwich TSSs with graphene-reinforced face sheets under axial loads. The study considered three graphene distribution laws for symmetric face sheets. Simplifying doubly curved coordinates using the Stein and McElman

assumption, they formulated nonlinear equations using Donnell shell theory and a two-parameter foundation model. The Galerkin method was applied for three buckling response states, determining expressions for load-deflection post-buckling curves.

By reviewing previous research on TSSs, it can be noted that there have been few studies done on the stability analysis of sandwich concave and convex auxetic-core TSSs with CNT-reinforced face sheets. This study explores and compares the stability characteristics of TSSs with sandwich auxetic cores, featuring different types of auxetic structures and face sheets reinforced with CNTs. The shells are subjected to radial pressure and are surrounded by Pasternak's elastic foundations. The fundamental governing equations are established by combining von Kármán-Donnell-type of kinematic nonlinearity with the Stein and McElman approximation, and subsequently solved using the Galerkin method .Numerical investigations confirm the notable influences of the different types of auxetic-core layers, parameters related to CNTs, geometrical parameters and the interaction with the elastic foundation on both the critical buckling load and the post-buckling behaviours of sandwich TSSs with different types of auxetic-core structures.

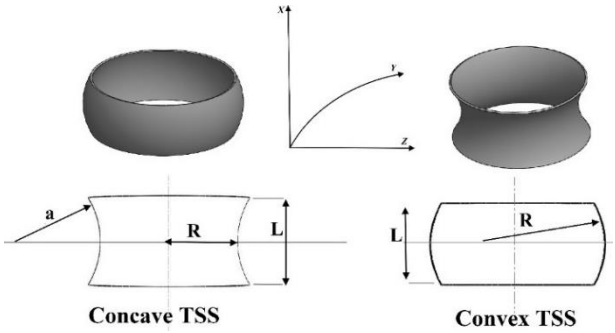

Fig. 1 Configuration of concave and convex TSSs

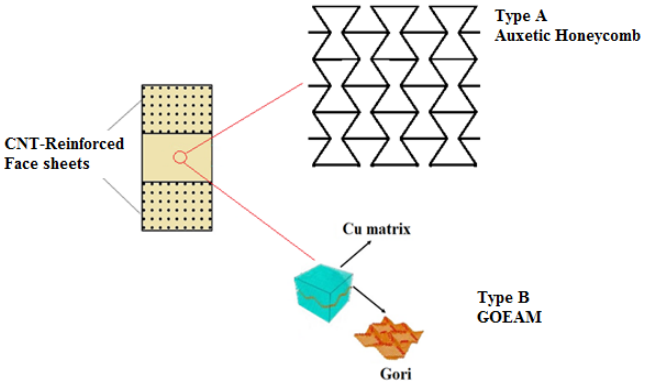

Fig. 2 Configuration of sandwich TSSs with CNT-reinforced face sheets featuring a core layer with: type A: re-entrant auxetic structure, and type B: GOEAM (GOEAM image taken from Zhao *et al.* (2022)

2. Auxetic-core sandwich TSSs with CNT-reinforced face sheets

2.1 Geometrical and material description

This study investigates sandwich TSSs with concave (exhibiting negative Gaussian curvature) and convex (exhibiting positive Gaussian curvature) configurations, as illustrated in Fig.1. The sandwich structure is composed of an auxetic-core layer and two face sheets, which are reinforced with CNTs with UD distribution type through the thickness, as shown in Fig.2. In the research, two distinct types of auxetic structures are considered the core of the sandwich composite, including: type A, characterized by a re-entrant auxetic structure, and type B, featuring GOEAM. A schematic representation of the sandwich TSSs featuring different types of auxetic materials and CNT-reinforced face sheets is shown in Fig. 2. In this paper, the extended rule of mixture is used for determining the elastic constants of orthotropic materials in the CNT-reinforced face sheets as follows (Shen 2011):

$$\begin{aligned} E_{11}^{\mathrm{CNTRC}} &= V_{ma}E_{ma} + \eta_1 V_{\mathrm{CNT}}E_{11}^{\mathrm{CNT}} \\ E_{22}^{\mathrm{CNTRC}} &= \frac{\eta_2}{\frac{V_{\mathrm{CNT}}}{E_{22}^{\mathrm{CNT}}} + \frac{V_{ma}}{E_{ma}}} \\ G_{12}^{\mathrm{CNTRC}} &= \frac{\eta_3}{\frac{V_{\mathrm{CNT}}}{G_{12}^{\mathrm{CNT}}} + \frac{V_{ma}}{G_{ma}}} \\ \nu_{12}^{\mathrm{CNTRC}} &= V_{ma}\,\nu_{ma} + V_{CNT}\,\nu_{12}^{\mathrm{CNT}} \end{aligned} \tag{1}$$

in which E_{11}^{CNT}, E_{22}^{CNT} and G_{12}^{CNT} represent the elastic moduli for the CNTs, while E_{ma} and G_{ma} denote the elastic moduli of the matrix material. Additionally, η_j (j=1, 2, 3) signifies the performance parameter for the CNTs, and V_{CNT} and V_{ma} are the volume fractions of the CNTs and the matrix, respectively, satisfying the relationship $V_{\mathrm{CNT}} + V_{ma} = 1$. Furthermore, the Poisson's ratios for the CNTs and matrix materials are referred to as ν_{12}^{CNT} and ν_{ma}, respectively.

2.2 Effective mechanical properties of various types of auxetic-core layer

In this study, two different types of auxetic structures are considered, including re-entrant auxetic structures (type A) and GOEAM (type B).

Type A (re-entrant auxetic structure):

The elastic constants of re-entrant auxetic material can be expressed as follows (Mahesh 2022)

$$\begin{aligned} E_{11}^{C} &= E_{ma}\frac{\lambda_3^3(\gamma_1 - \sin\,\theta)}{\cos\,\theta[1 + (\tan^2\,\theta + \lambda_1\sec^2\,\theta)\,\lambda_3^2]} \\ E_{22}^{C} &= E_{ma}\frac{\gamma_3^3}{\cos\theta(\lambda_1 - \sin\theta)(\tan^2\theta + \lambda_3^2)} \\ \nu_{12}^{C} &= -\frac{\sin\theta(1-\lambda_3^2)(\lambda_1 - \sin\theta)}{[1 + (\lambda_1\sec^2\theta + \tan^2\theta)\,\lambda_3^2]\cos^2\theta} \\ \nu_{21}^{C} &= -\frac{\sin\,\theta(1-\lambda_3^2)}{(\tan^2\,\theta + \lambda_3^2)(\lambda_1 - \sin\,\theta)} \\ G_{12}^{C} &= E_{ma}\frac{\lambda_3^3}{\gamma_1(1+2\lambda_1)\cos\theta} \end{aligned} \tag{2}$$

$$\rho^C = \rho \frac{\lambda_3(\lambda_1+2)}{2\cos\alpha(\lambda_1-\sin\alpha)}$$

where λ_1 and λ_3 are the length ratios of the auxetic rib Furthermore, methyl methacrylate (PMMA) is used in the fabrication of the auxetic-core layer.

Type B (GOEAM)

The mechanical characteristics of GOEAM, including Young's modulus E_c, Poisson's ratio ν_c, coefficient of thermal expansion α_c, and density ρ_c, in GOEAM which developed by Zhao *et al*. (2022), can be presented as follows:

$$\begin{aligned} E_c &= \frac{1+\xi\eta\, V_{Gr}}{1-\eta V_{Gr}} E_{Cu} \times f_E(H_{Gr}, V_{Gr}, T) \\ \nu_c &= (\nu_{Gr}V_{Gr} + \nu_{Cu}V_{Cu}) \times f_\nu(H_{Gr}, V_{Gr}, T) \\ \alpha_c &= (\alpha_{Gr}V_{Gr} + \alpha_{Cu}V_{Cu}) \times f_\alpha(V_{Gr}, T) \\ \rho_c &= (\rho_{Gr}V_{Gr} + \rho_{Cu}V_{Cu}) \times f_\rho(V_{Gr}, T) \end{aligned} \tag{3}$$

where η and ξ denote the material coefficient and size coefficient, respectively. Furthermore, f_E, f_ν, f_α and f_ρ are the modification functions, which are provided in (Zhao *et al*. 2022). Also, T_0 is equivalent to 300 *K*, and *T* represents the ambient temperature.

3. Fundamental equations

The fundamental equations describing the mechanical properties of TSSs considering various types of auxetic cores and CNT-reinforced composite face sheets under external load, as presented in this study, can be derived from the von Karman-Donnell theory. Fig. 1 illustrates how TSSs are located within a complex coordinate system with doubly curved geometry. The shallowness of the TSSs along the meridian allows the application of the Stein and McElman approximation (Stein and McElman 1965), leading to a simplification of the governing equations for the shells.

The strain at the mid-surface of the shells is presented as (Stein and McElman 1965):

$$\begin{aligned} \varepsilon_x^0 &= \frac{\partial u}{\partial x} + \left(\frac{\partial w}{\partial x}\right)^2 - \frac{w}{a} \\ \varepsilon_x^0 &= \frac{\partial v}{\partial x} + \left(\frac{\partial w}{\partial y}\right)^2 - \frac{w}{R} \\ \gamma_{xy}^0 &= \frac{\partial u}{\partial y} + \frac{\partial v}{\partial x} + \frac{\partial w}{\partial x}\frac{\partial w}{\partial y} \end{aligned} \tag{4}$$

where u, v, and w are displacement components in the x, y, and z directions, respectively. Hooke's law for linear elastic materials is utilized to establish the stress-strain relations for orthotropic layers, as (Reddy 2003):

$$\begin{bmatrix}\sigma_x\\ \sigma_y\\ \sigma_{xy}\end{bmatrix} = \begin{bmatrix}Q_{11} & Q_{12} & 0\\ Q_{12} & Q_{22} & 0\\ 0 & 0 & Q_{66}\end{bmatrix}\begin{bmatrix}\varepsilon_x\\ \varepsilon_y\\ \gamma_{xy}\end{bmatrix} \tag{5}$$

where

$$\begin{aligned} Q_{11} &= \frac{E_{11}}{1-\nu_{12}\nu_{21}}, \quad Q_{12} = \frac{E_{11}\nu_{21}}{1-\nu_{12}\nu_{21}} \\ Q_{22} &= \frac{E_{22}}{1-\nu_{12}\nu_{21}}, Q_{66} = G_{12} \end{aligned} \tag{6}$$

By integrating Eq. (8) across the shell's thickness, it becomes possible to derive the internal forces within sandwich TSSs as follows:

$$\begin{bmatrix}N_x\\ N_y\\ N_{xy}\\ M_x\\ M_y\\ M_{xy}\end{bmatrix} = \begin{bmatrix}A_{11} & A_{12} & 0 & 0 & 0 & 0\\ A_{12} & A_{22} & 0 & 0 & 0 & 0\\ 0 & 0 & A_{66} & 0 & 0 & 0\\ 0 & 0 & 0 & D_{11} & D_{12} & 0\\ 0 & 0 & 0 & D_{12} & D_{22} & 0\\ 0 & 0 & 0 & 0 & 0 & D_{66}\end{bmatrix}\begin{bmatrix}\varepsilon_x^0\\ \varepsilon_y^0\\ \gamma_{xy}^0\\ -w_{,xx}\\ -w_{,yy}\\ -2w_{,xy}\end{bmatrix} \tag{7}$$

where A_{ij}, D_{ij} are the total stiffnesses of the sandwich TSSs.

The equilibrium equations for sandwich TSSs, while considering Winkler-Pasternak elastic foundation (with foundation stiffness coefficients denoted as K_1, K_2), can be expressed as follows (Tien *et al*. 2022):

$$\begin{aligned} &N_{x,x} + N_{xy,y} = 0 \\ &N_{xy,x} + N_{y,y} = 0 \\ &M_{x,xx} + M_{y,yy} + 2M_{xy,xy} + N_x w_{,xx} \\ &+N_y w_{,yy} + 2N_{xy} w_{,xy} + \frac{N_x}{a} + \frac{N_y}{R} \\ &= -q_0 + K_1 w - K_2\left(w_{,xx} + w_{,yy}\right) \end{aligned} \tag{8}$$

The Airy stress function $\varsigma(x,y)$ may be introduced as (Nam *et al*. 2022):

$$\phi_{,yy} = N_x,\ \phi_{,xx} = N_y,\ \phi_{,xy} = -N_{xy} \tag{9}$$

It is evident that when three conditions (12) are met, the first two equations in Eq. (11) are also satisfied. By substituting Eqs. (10) and (12) into the last equation of Eq. (11), the equilibrium equations can be derived as (Nam 2022):

$$\begin{aligned} &D_{11}w_{,xxxx} + D_{22}w_{,yyyy} + (D_{12} + D_{21} + 4D_{66})w_{,xxyy} \\ &-\frac{1}{R}\phi_{,xx} - \frac{1}{a}\phi_{,yy} - \phi_{,yy}w_{,xx} - \phi_{,xx}w_{,yy} + 2\phi_{,xy}w_{,xy} \\ &+K_1 w - K_2\left(w_{,xx} + w_{,yy}\right) - q_0 = 0 \end{aligned} \tag{10}$$

From Eq. (13) the deformation compatibility equation can be obtained as:

$$\begin{aligned} &\varepsilon_{x,yy}^0 + \varepsilon_{y,xx}^0 - \gamma_{xy,xy}^0 \\ &= -\frac{1}{R}w_{,xx} - \frac{1}{a}w_{,yy} + w_{,xy}^2 - w_{,xx}w_{,yy} \end{aligned} \tag{11}$$

Substituting Eq. (10) into the compatibility Eq. (14) yields:

$$\begin{aligned} &\bar{C}_{11}\,\phi_{,xxxx} + \bar{C}_{22}\,\phi_{,yyyy} + (\bar{C}_{66} - 2\bar{C}_{12})\,\phi_{,xxyy} \\ &-w_{,xy}^2 + w_{,xx}w_{,yy} + \frac{1}{R}w_{,xx} + \frac{1}{a}w_{,yy} = 0 \end{aligned} \tag{12}$$

where:

$$\bar{C}_{11}=\frac{A_{11}}{\Delta},\ \bar{C}_{22}=\frac{A_{22}}{\Delta},\ \bar{C}_{12}=\frac{A_{12}}{\Delta},$$
$$\bar{C}_{66}=\frac{1}{A_{66}},\ \Delta=A_{11}A_{22}-A_{12}^2$$

Applying the closed condition to the closed shell yields (Huang and Han, 2009):

$$\int_0^{2\pi R}\int_0^{L} v_{,y}dxdy = \int_0^{2\pi R}\int_0^{L}\left(\varepsilon_y^0+\frac{w}{R}-\frac{1}{2}w_{,y}^2\right)dxdy=0 \tag{13}$$

The governing Eqs. (13, 15, 16) can be utilized for exploring the stability behavior of sandwich TSSs.

4. Solution procedure

In this article, the stability analysis of radially-loaded sandwich TSSs is investigated. The face sheets are reinforced with CNTs, while the effects of various types of auxetic structures are examined and compared as the core of the sandwich composite. The analysis is conducted considering simply supported boundary conditions as follows:

$$w=0, N_x=0, M_x=0 \tag{14}$$

The deflection of the shells can be approximated as (Huang and Han 2009):

$$w=\xi_0+\xi_1\sin\frac{m\pi x}{L}\sin\frac{ny}{R}+\xi_2\sin^2\frac{m\pi x}{L} \tag{15}$$

where m and n represent the longitudinal and radial buckling modes, ξ_0 is the pre-buckling deflection amplitude, and ξ_1,ξ_2 are the linear and nonlinear post-buckling deflection amplitudes, respectively. The boundary condition (17) is approximately satisfied by the three-term deflection expression (14). By substituting Eq. (18) into Eq. (15), the stress function can be obtained as (Nam 2022)

$$\phi=\phi_1\cos\frac{2m\pi x}{L}+\phi_2\cos\frac{2ny}{R}-\phi_3\sin\frac{m\pi x}{L}\sin\frac{ny}{R} +\phi_4\sin\frac{3m\pi x}{L}\sin\frac{ny}{R}-\sigma_{0y}h\frac{x^2}{2} \tag{16}$$

where the ϕ_i expressions (i =1 to 4) are provided in (Tien *et al*. 2022). By substituting the stress function (19) and deflection Eq. (18) in Eq. (15), applying the Galerkin method, and taking into consideration the Eq. (16), the equilibrium equations, which are expressed algebraically, can be derived as:

$$\xi_0=\frac{S_{32}}{2S_{31}}\xi_1^2-\frac{1}{2}\xi_2+\frac{S_{33}}{2S_{31}}q_0 \tag{17}$$

$$S_{11}+S_{12}\xi_0+S_{13}\xi_1^2+S_{14}\phi_2+S_{15}\xi_2^2-S_{16}q_0=0 \tag{18}$$

$$\xi_1=\sqrt{-\frac{S_{23}\xi_2}{S_{22}+\xi_2 S_{21}}} \tag{19}$$

where the expressions of A, B, D and S_{ij} are presented in (Tien *et al*. 2022).

The relation between load and nonlinear amplitude can be determined by solving Eqs. (20)-(22) as:

$$q=\left\{\begin{matrix} S_{11}+\left(S_{14}-\frac{S_{12}}{2}\right)\xi_2-\frac{S_{12}S_{32}S_{23}\xi_2}{2S_{31}(S_{21}+S_{22}\phi_2)} \\ -\frac{S_{13}S_{23}\xi_2}{S_{21}+S_{22}\xi_2}+S_{15}\xi_2^2 \end{matrix}\right\} \times\left(\frac{2S_{31}}{2S_{16}S_{31}-S_{12}S_{33}}\right) \tag{20}$$

As ξ_2 tends to zero, the upper buckling load of the shells can be calculated as:

$$q_{\max}=\frac{2S_{11}S_{31}}{2S_{31}S_{16}-S_{12}S_{33}} \tag{21}$$

By utilizing Eq. (18), the maximum deflection of the shell can be represented as:

$$W_{\max}=\xi_0+\xi_1+\xi_2 \tag{22}$$

By substituting Eqs. (24) and (25) into Eq. (25), the relationship between maximum deflection and nonlinear amplitude can be obtained, as follows:

$$W_{\max}=\frac{\xi_2}{2}-\frac{S_{32}S_{23}\xi_2}{2S_{31}(S_{21}+S_{22}\xi_2)} +\left(-\frac{S_{23}\xi_2}{S_{21}+S_{22}\xi_2}\right)^{1/2}+\frac{S_{33}}{2S_{31}}q \tag{23}$$

The post-buckling curves ($q-W_{\max}/h$) can be achieved by combining Eqs. (23) and (26).

5. Numerical results and discussion

In comparison with Shen *et al*.'s research (2011), which employs the nonlinear higher-order shear deformation theory, the critical radial buckling loads of CNTRC cylindrical shells in Table. 1 are verified. Acceptable agreements are found in this study when the validation cases are examined for various values of $\bar{Z}=\frac{L^2}{Rh}$. The numerical investigations involving the PMMA matrix and CNTs are presented, as discussed by Shen *et al*.'s research (2011). Also, the mechanical characteristics of Cu and graphene at 300 K, which were used in the GOEAM core, are according to Zhao *et al*.'s report (2022). Furthermore, the GOri is distributed uniformly throughout the shell thickness with a weight fraction of 2.5 wt%, while the GOri folding degree is maintained at a constant value of 100%.

A comparison of the buckling loads for convex and concave auxetic-core TSSs, where the face sheets are circumferentially and longitudinally reinforced with CNTs, is shown in Table 2. Auxetic materials of both types—type B, as used in this work, and type A, as studied by Tien *et al*. (2022)—are considered. The findings suggest that incorporating a higher proportion of Gori into the shells

Table 1 Validation of critical radial buckling load q_{cr} (kPa) for CNT-reinforced cylindrical shells ($h = 1$ mm, $R/h = 100$)

L^2/Rh	V_{CNT}	Shen	Present
100	0.12	42.68(1; 10)	42.8264(1; 10)
	0.17	70.06(1; 10)	70.2862(1; 10)
	0.28	84.34(1; 10)	84.6711(1; 10)
300	0.12	23.40(1; 8)	23.4506(1; 8)
	0.17	38.98(1; 8)	39.0591(1; 8)
	0.28	45.11(1; 8)	45.2221(1; 8)

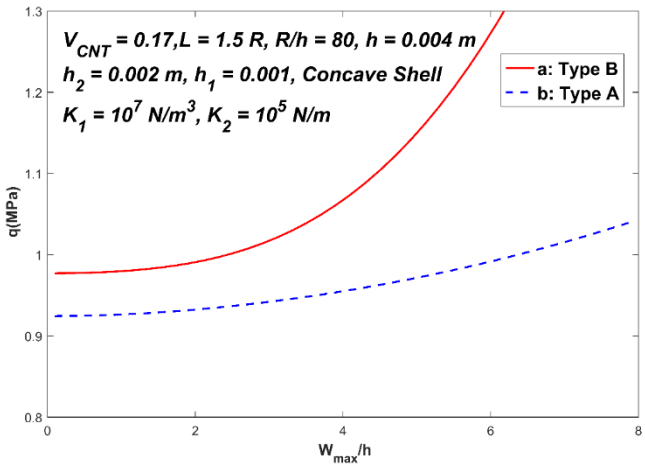

Fig. 1 Influence of different types of auxetic cores on the post-buckling behavior of the concave TSSs

Table 2 Comparative analysis of radial critical buckling load of convex and concave TSSs between two different types of auxetic cores $\left(\text{MPa}\ K_1 = \frac{10^7\ \text{N}}{\text{m}^3} K_2 = \frac{10^5\ \text{N}}{\text{m}} R/h = 80, L = 1.5R\ \ h = 0.004\ \text{m}, h_2 = 0.002\ \text{m}\ h_1 = 0.001\ \text{m}\right)$

CNT direction	V_{CNT}	Type A (Tien *et al*. 2022)	Type B (present)
Convex shell segments ($a = 4R$) x-direction	0.12	0.558(1; 12)	1.1270(1; 14)
	0.17	0.620(1; 11)	1.2746(1; 14)
	0.28	0.653(1; 11)	1.4418(1; 15)
y-direction	0.12	0.923(1; 5)	2.080(1; 8)
	0.17	1.133(1; 5)	2.5037(1; 8)
	0.28	1.411(1; 4)	3.1416(1; 7)
Concave shell segment($a = -4R$)			
x-direction	0.12	0.520(1; 10)	0.688(1; 4)
	0.17	0.543(1; 8)	0.7043(1; 4)
	0.28	0.557(1; 8)	0.7242(1; 4)
y-direction	0.12	0.824(1; 4)	0.8754(1; 4)
	0.17	0.924(1; 4)	0.9772(1; 4)
	0.28	1.121(1; 4)	1.1745(1; 4)

significantly increases buckling loads. This can be attributed to transforming GOEAM-core into auxetic metamaterials. As more GOri is integrated into the matrix, this transformation leads to a more significant Young's modulus and auxeticity. As a result, the shells exhibit higher stiffness, thereby enhancing their ability to withstand buckling loads.

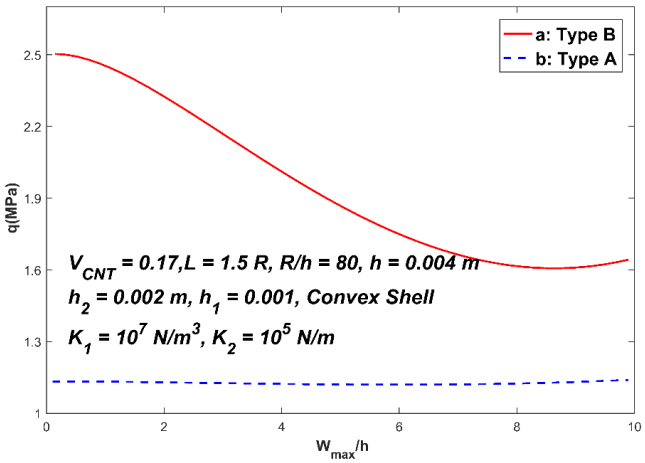

Fig. 2 Influence of different types of auxetic cores on the post-buckling behavior of the convex TSSs

Table 3 Effects of different R/h ratios on the critical buckling loads of the auxetic-core shells (MPa, $K_1 = 10^7$ N/m^3, $K_2 = 10^5$ N/m, $L = 1.5R$, $h = 0.004$ m, $h_2 = 0.002$ m, $h_1 = 0.001$ m, $V_{CNT} = 0.28$, y-direction)

	R/h Ratio	Type A	Type B
Convex toroidal shell	60	2.3028(1; 4)	5.66(1; 6)
	80	1.4113(1; 4)	3.1416(1; 7)
	100	0.9913(1; 5)	2.0393(1; 8)
Concave toroidal shell	60	1.6907(1; 3)	2.0310(1; 4)
	80	1.1211(1; 4)	1.1745(1; 4)
	100	0.8381(1; 4)	0.8685(1: 4)

Furthermore, the elastic modulus is notably higher in the direction of CNTs compared to the orthogonal direction. The findings also indicate that the buckling loads of the shells reinforced circumferentially were higher than those of the shells reinforced longitudinally. This difference can be attributed to the superior efficiency of the elastic modulus in the circumferential direction. Moreover, the shells reinforced longitudinally had smaller buckling modes compared to the shells reinforced in the x-direction.

The post-buckling behavior of concave and convex TSSs is illustrated in Figs. 1-2, highlighting the impact of different core types. Notably, the post-buckling curves of type-B auxetic-core shells surpass those of type-A shells in both concave and convex scenarios, which emphasizes the importance of core types in influencing the structural stability of TSSs.

Table 3 presents the effects of different R/h ratios on the critical buckling loads of concave and convex shell segments for both cases of type-A and type-B auxetic-core layers with face sheets reinforced with CNTs. It is evident that the critical radial buckling load of the shells is significantly influenced by the *R/h* ratio.

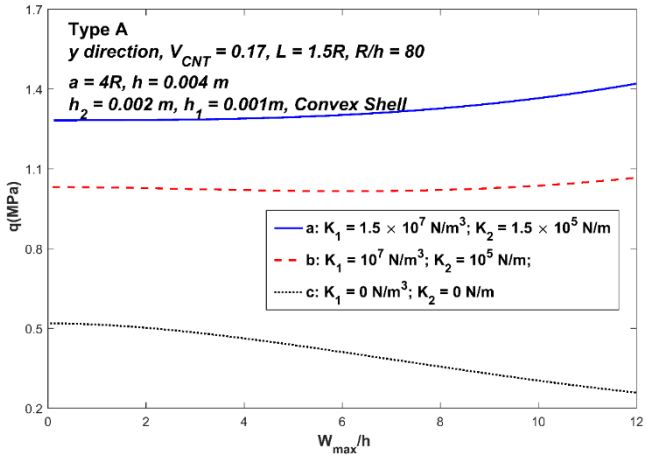

Fig. 3 Influence of elastic foundation on the post-buckling behavior in type-B auxetic-core convex TSSs

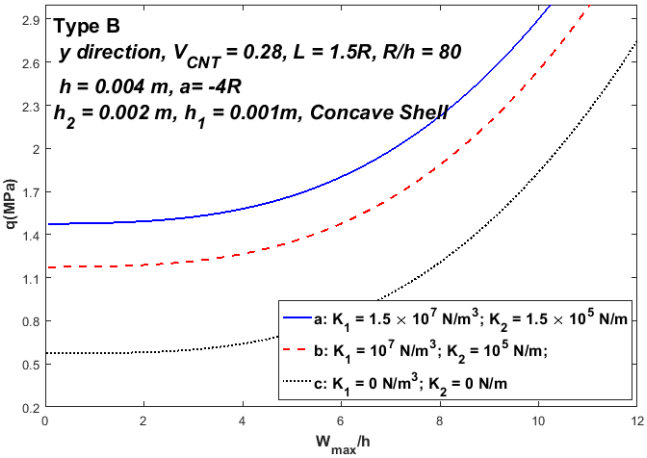

Fig. 4 Influence of elastic foundation on the post-buckling behavior in type-B auxetic-core concave TSSs

The influence of foundation stiffnesses on both the post-buckling curve and the critical buckling load of shells is shown in Figs. 3-4. The studies obtained demonstrate that the stiffness of the foundations significantly influences the buckling loads and post-buckling curves of the TSSs. In both the convex and concave shells, the buckling mode remains unchanged when the foundation stiffness varies. An additional noteworthy finding is that there is a significant decrease in snap-through buckling as foundation parameters increase.

6. Conclusions

This study presents a comparison between two types of auxetic-core structures on the stability of sandwich concave and convex TSSs with CNT-reinforced face sheets under radial load. A novel design featuring auxetic-core sandwich TSSs with CNT-reinforced face sheets is introduced, along with an analytical approach to explore the stability of shells under external load. Numerical investigations yield noteworthy findings:

• The critical radial buckling load is highest in GOEAM-core sandwich TSSs with face sheets reinforced circumferentially by CNTs.

• The critical radial buckling load of TSSs is significantly influenced by both the direction of CNT and the presence of different types of auxetic structures.

• The direction of CNTs and the type of auxetic core have a substantial impact on the critical radial buckling load of TSSs.

• The phenomena of snap-through may be seen quite well in the case of convex shells, whereas the concave shell does not exhibit this behavior.

• GOEAM serves as an excellent core material, providing a distinct advantage for achieving enhanced tunability in the stability characteristics of shell structures through GOri parameters.

• Lastly, an elastic finding plays a significant role in the stability of sandwich TSSs under radial load.

References

Dabbagh, A., Golpaygani Sani, S. and Ebrahimi, F. (2023), "Piezoelectrically controlled wave propagation in laminates with auxetic core: Transient analysis incorporated with electrical stability monitoring", *Eur. Phys. J. Plus*, **138**(9), 1-21. https://doi.org/10.1140/epjp/s13360-023-04405-3

Ebrahimi, F. (2024), *Mechanics of Auxetic Materials and Structures*, CRC Press.

Ebrahimi, F. and Dadashi, M. (2023), "Composite cylindrical shells with auxetic core on elastic foundation: A nonlinear dynamic analysis", *Structures*, **57**, 105170. https://doi.org/10.1016/j.istruc.2023.105170

Ebrahimi, F. and Parsi, M. (2023), "Wave propagation analysis of functionally graded graphene origami-enabled auxetic metamaterial beams resting on an elastic foundation", *Acta Mechanica*, **234**(12), 6169-6190. http://doi.org/10.1007/s00707-023-03705-0

Ebrahimi, F. and Ahari, M.F. (2024), "On the buckling of meta-graphene-origami-enabled magnetostrictive nanoplates under temperature gradient", *Acta Mechanica*, 1-18. http://doi.org/10.1007/s00707-024-03861-x

Ebrahimi, F. and Dabbagh, A. (2022), *Mechanics of Multiscale Hybrid Nanocomposites*, Elsevier.

Ebrahimi, F. (2015), *Graphene: New Trends and Developments*, BoD–Books on Demand.

Ebrahimi, F. and Dabbagh, A. (2020), *Mechanics of Nanocomposites: Homogenization and Analysis*. CRC Press.

Ebrahimi, F., Dabbagh, A. and Civalek, Ö. (2019), "Vibration analysis of magnetically affected graphene oxide-reinforced nanocomposite beams", *J. Vib. Control*, **25**(23-24), 2837-2849. https://doi.org/10.1177/10775463198610

Ebrahimi, F. and Barati, M.R. (2019), "Vibration analysis of biaxially compressed double-layered graphene sheets based on nonlocal strain gradient theory", *Mech. Adv. Mater. Struct.*, **26**(10), 854-865. https://doi.org/10.1080/15376494.2018.1430267

Ebrahimi, F., Hosseini, S.H.S. and Bayrami, S.S. (2019), "Nonlinear forced vibration of pre-stressed graphene sheets subjected to a mechanical shock: an analytical study", *Thin Wall. Struct.*, **141**, 293-307. http://doi.org/10.1016/j.tws.2019.04.038

Ebrahimi, F., Nouraei, M. and Dabbagh, A. (2020), "Modeling

vibration behavior of embedded graphene-oxide powder-reinforced nanocomposite plates in thermal environment", *Mech. Based Des. Struct.*, **48**(2), 217-240. http://doi.org/10.1080/15397734.2019.1660185

Ebrahimi, F. and Barati, M.R. (2018), "Damping vibration analysis of graphene sheets on viscoelastic medium incorporating hygro-thermal effects employing nonlocal strain gradient theory", *Compos. Struct.*, **185**, 241-253. https://doi.org/10.1016/j.compstruct.2017.10.021

Ebrahimi, F. and Dabbagh, A. (2019), *Wave Propagation Responses of Double-Layered Graphene Sheets in Hygrothermal Environment, Handbook of Graphene, Volume 8: Technology and Innovations*, 289. https://doi.org/10.12989/sem.2018.65.6.645

Hieu, P.T. and Tung, H.V. (2020), "Postbuckling behavior of carbon-nanotube-reinforced composite toroidal shell segments subjected to thermomechanical loadings", *AIAA J.*, **58**(7), 3187-3198. http://doi.org/10.2514/1.J059055

Huang, H. and Han, Q. (2009), "Nonlinear elastic buckling and postbuckling of axially compressed functionally graded cylindrical shells", *Int. J. Mech. Sci.*, **51**(7), 500-507. https://doi.org/10.1016/j.ijmecsci.2009.05.002

Kamrava, S., Mousanezhad, D., Ebrahimi, H., Ghosh, R. and Vaziri, A. (2017), "Origami-based cellular metamaterial with auxetic, bistable, and self-locking properties", *Sci. Rep.*, **7**(1), 46046. https://doi.org/10.1038/srep46046

Kolken, H.M. and Zadpoor, A.A. (2017), "Auxetic mechanical metamaterials", *RSC Adv.*, **7**(9), 5111-5129. https://doi.org/10.1039/C6RA27333E

Kiani, Y. (2018a), "NURBS-based isogeometric thermal post-buckling analysis of temperature dependent graphene reinforced composite laminated plates", *Thin Wall. Struct.*, **125**, 211-219. https://doi.org/10.1016/j.tws.2018.01.024

Kiani, Y. (2018b), "Isogeometric large amplitude free vibration of graphene reinforced laminated plates in thermal environment using NURBS formulation", *Comput. Meth. Appl. Mech. Eng.*, **332**, 86-101. https://doi.org/10.1016/j.cma.2017.12.015

Mahesh, V. (2022), "Nonlinear free vibration of multifunctional sandwich plates with auxetic core and magneto-electro-elastic facesheets of different micro-topological textures: FE approach", *Mech. Adv. Mater. Struct.*, **29**(27), 6266-6287. http://doi.org/10.1080/15376494.2021.1974619

Mahinzare, M., Rastgoo, A. and Ebrahimi, F. (2024), "Nonlinear vibration of FG graphene origami auxetic sandwich plate including smart hybrid nanocomposite sheets", *J. Eng. Mech.*, **150**(4), 04024007. https://doi.org/10.1061/JENMDT.EMENG-7398

Mahinzare, M., Rastgoo, A. and Ebrahimi, F. (2023), "On nonlinear vibration of piezo-electrically multi-scale hybrid nanocomposite sandwich plate including an auxetic core based on HSDT", *Int. J. Struct. Stabil. Dyn.*, **24**(5), 2450069. https://doi.org/10.1142/S021945542450069X

Nam, V.H., Duc, V.M., Doan, C.V., Xuan, N.T. and Phuong, N.T. (2022), "Nonlinear postbuckling behavior of auxetic-core toroidal shell segments with Graphene reinforced face sheets under axial loads", *Arch. Mech.*, **74**. http://doi.org/10.24423/aom.3957

Nguyen, T.P., Vu, M.D., Dang, T.D., Cao, V.D., Pham, T.H. and Vu, H.N. (2023), "An analytical approach of nonlinear buckling behavior of torsionally loaded auxetic core toroidal shell segments with graphene reinforced polymer coatings", *Adv. Compos. Mater.*, **32**(3), 400-418. http://doi.org/10.1080/09243046.2022.2110661

Phuong, N.T., Van Doan, C., Duc, V.M., Giang, N.T. and Nam, V.H. (2023), "Analytical solution for nonlinear buckling of convex and concave auxetic-core toroidal shell segments with graphene-reinforced face sheets subjected to radial loads", *Arch. Appl. Mech.*, **93**(2), 621-634. https://doi.org/10.1007/s00419-022-02288-x

Reddy, J.N. (2003), *Mechanics of Laminated Composite Plates and Shells: Theory and Analysis*. CRC press.

Seyfi, A., Teimouri, A. and Ebrahimi, F. (2021), "Scale-dependent torsional vibration response of non-circular nanoscale auxetic rods", *Waves Random Complex Med.*, 1-17. http://doi.org/10.1080/17455030.2021.1990441

Shen, H.S. and Xiang, Y. (2018), "Postbuckling behavior of functionally graded graphene-reinforced composite laminated cylindrical shells under axial compression in thermal environments", *Comput. Meth. Appl. Mech. Eng.*, **330**, 64-82. http://doi.org/10.1016/j.cma.2017.10.022

Shen, H.S. (2011), "Postbuckling of nanotube-reinforced composite cylindrical shells in thermal environments, Part II: Pressure-loaded shells", *Compos. Struct.*, **93**(10), 2496-2503. http://doi.org/10.1016/j.compstruct.2011.04.005

Shen, H.S. (2014), "Torsional postbuckling of nanotube-reinforced composite cylindrical shells in thermal environments", *Compos. Struct.*, **116**, 477-488. http://doi.org/10.1016/j.compstruct.2014.05.039

Shen, H.S. and Xiang, Y. (2018), "Postbuckling of functionally graded graphene-reinforced composite laminated cylindrical shells subjected to external pressure in thermal environments", *Thin Wall. Struct.*, **124**, 151-160. https://doi.org/10.1016/j.tws.2017.12.005

Shen, H.S., Xiang, Y. and Lin, F. (2017), "Nonlinear bending of functionally graded graphene-reinforced composite laminated plates resting on elastic foundations in thermal environments", *Compos. Struct.*, **170**, 80-90. https://doi.org/10.1016/j.compstruct.2017.03.001

Sofiyev, A.H. and Kuruoglu, N.U.R.İ. (2022), "Buckling analysis of shear deformable composite conical shells reinforced by CNTs subjected to combined loading on the two-parameter elastic foundation", *Defence Technol.*, **18**(2), 205-218. http://doi.org/10.1016/j.dt.2020.12.007

Stein, M. and McElman, J.A. (1965), "Buckling of segments of toroidal shells", *AIAA J.*, **3**(9), 1704-1709.

Van Tien, N., Duc, V.M., Nam, V.H., Phuong, N.T., Ho, L.S., Dong, D.T., Ly, L.N., Hung, D. and Minh, T.Q. (2022), "Nonlinear postbuckling of auxetic-core sandwich toroidal shell segments with CNT-reinforced face sheets under external pressure", *Int. J. Struct. Stabil. Dyn.*, **22**(1), 2250006. http://doi.org/10.1142/S0219455422500067

Zhai, Z., Wu, L. and Jiang, H. (2021), "Mechanical metamaterials based on origami and kirigami", *Appl. Phys. Rev.*, **8**(4). http://doi.org/10.1063/5.0051088

Zhao, S., Zhang, Y., Zhang, Y., Yang, J. and Kitipornchai, S. (2022), "Vibrational characteristics of functionally graded graphene origami-enabled auxetic metamaterial beams based on machine learning assisted models", *Aerosp. Sci. Technol.*, **130**, 107906. https://doi.org/10.1016/j.ast.2022.107906

Zhao, S., Zhang, Y., Wu, H., Zhang, Y. and Yang, J. (2022), "Functionally graded graphene origami-enabled auxetic metamaterial beams with tunable buckling and postbuckling resistance", *Eng. Struct.*, **268**, 114763. https://doi.org/10.1016/j.engstruct.2022.114763

Zhao, S., Zhang, Y., Zhang, Y., Zhang, W., Yang, J. and Kitipornchai, S. (2022), "Genetic programming-assisted micro-mechanical models of graphene origami-enabled metal metamaterials", *Acta Materialia*, **228**, 117791. https://doi.org/10.1016/j.actamat.2022.117791

AT